Colloids and Surfaces B: Biointerfaces 184 (2019) 110500

Contents lists available at ScienceDirect

Colloids and Surfaces B: Biointerfaces

journal homepage: www.elsevier.com/locate/colsurfb

Nanorods to hexagonal nanosheets of CuO-doped manganese oxide nanostructures for higher electrochemical supercapacitor performance

H.M. Yadav[a], G.S. Ghodake[b], D.-Y. Kim[b], Sivalingam Ramesh[c], N.C. Maile[d], D.S. Lee[d], S.K. Shinde[b,*]

[a] Department of Energy and Materials Engineering, Dongguk University, 04620, South Korea
[b] Department of Biological and Environmental Science, College of Life Science and Biotechnology, Dongguk University, 32 Dongguk-ro, Biomedical Campus, Ilsandong-gu, Siksa-dong, 10326, Goyang-si, Gyeonggi-do, South Korea
[c] Department of Mechanical, Robotics and Energy Engineering, Dongguk University –Seoul, Seoul, 04620, South Korea
[d] Department of Environmental Engineering, Kyungpook National University, 80 Daehak-ro, Buk-gu, Daegu, 41566, South Korea

ARTICLE INFO

Keywords:
Nanorod
Nanosheets
SILAR method
Supercapacitor
CuO/Mn_2O_3 thin films

ABSTRACT

In this work, the extraordinary properties of CuO addition on the morphology and supercapacitive performance of Mn_2O_3 electrodes were demonstrated. Concisely, CuO/Mn_2O_3 thin films were prepared by an easy and inexpensive successive ionic layer adsorption and reaction (SILAR) method. The prepared thin films were characterized by various sophisticated physiochemical systems. The results demonstrated formation of Mn_2O_3 thin films with noteworthy morphological alteration upon introduction of CuO. Furthermore, a significant effect of CuO introduction was observed on the electrocatalytic properties of the nanostructured Mn_2O_3 electrodes. At 3% CuO doping, the Mn_2O_3 electrodes displayed the maximum specific capacitance owing to formation of nanoplate-like structures. The enhanced specific capacitance attained for 3% CuO doping in the Mn_2O_3 electrode was 500 F/g at 5 mV/s in a 3 M KOH electrolyte. All results confirmed the plausible potential of the CuO/Mn_2O_3 electrode for supercapacitor applications.

1. Introduction

In recent years, supercapacitors have emerged as good candidates for different energy storage applications owing their excellent power density, extensive cycle life, high rate capability, high reversibility, and extremely fast charging/discharging [1]. The increasing energy demands and the consequent environmental impact have encouraged a search for alternative clean and sustainable energy storage technologies with high efficiency and excellent performance [2]. Accordingly, considerable attempts have been made to find a suitable electrode materials with decent capacitive features analogous to those of NiO, CoOx, CuO, MnO_2, Fe_3O_4, etc. [3–7]. Among the different transition metal oxides, manganese oxide has attracted attention because of its low cost, environmental friendliness, high energy density, universal abundance, high theoretical capacity (1370 F/g), and excellent electrochemical properties for applications in supercapacitors and use as an electrocatalyst in basic reagents for the oxygen reduction reaction (ORR) [2,8–10].

Different strategies have been proposed to boost the electrochemical properties of manganese oxides. The electrochemical features of a substance are mainly determined by their electronic structure. Extra energy states can be introduced to metal oxides by doping other materials to alter their electronic characteristics [8]. The most prominent method to enhance the specific capacity of metal oxide is the addition of metal ions to develop desired mixed metal compounds [11]. The doping of heteroatoms can strengthen the pseudocapacitive and electrochemical properties of manganese oxides [8]. Among different metal dopants, the copper cation is considered as a superior dopant because of its electrical conductivity, environmentally benign nature, and low cost [2,12]. P-type materials such as CuO and manganese oxides with a tiny band gap (E_g = 1.2 eV) are considered dynamic materials in batteries and supercapacitors [2]. Copper-based manganese oxides material has been used as catalyst for the oxidation of CO [13], hydrogenation reaction [14], oxidative decomposition of ethyl acetate [15], and oxidation of 5-hydroxymethylfurfural [16], Fe, and Mn doped CuSe [17].

Recently, Li et al. prepared various transition metal (Fe, Co, Ni, and V) ion-doped MnO_2 on carbon for the ORR and supercapacitor applications. They prepared manganese oxides nanosheets by a redox reaction between the macroporous carbon and a $KMnO_4$ solution. They found that the electrochemical performance can be improved by doping

* Corresponding author.
E-mail address: surendrashinde@dongguk.edu (S.K. Shinde).

https://doi.org/10.1016/j.colsurfb.2019.110500
Received 29 July 2019; Received in revised form 3 September 2019; Accepted 10 September 2019
Available online 11 September 2019
0927-7765/

with appropriate elements [8]. In another study, Davis et al. showed that the current density can be enhanced using Cu-MnO_2 nanowires because it can facilitate equilibrium of O_2 adsorption on their exterior [9]. Zhang et al. prepared CuO/MnO_2 core–shell structures by hydrothermal synthesis that exhibited a promising specific capacitance of 228 F/g [18]. Chen et al. [19] anchored CuO nanowires on porous MnO_2 nanosheets by hydrothermal synthesis. The CuO@MnO_2 electrode showed a specific capacitance of 343.9 F/g at a current density of 0.25 A/g. Huang et al. developed hierarchical CuO@MnO_2 core–shell heterostructures, also by the hydrothermal method. The complex heterostructures showed a high specific capacitance of 276 F/g at a current density of 0.6 A/g [10]. Poonguzhali et al. [11] synthesized Cu-MnO_2 nanocrystals by precipitation with different doping contents (0.025–0.125 M). Cu-doping in MnO_2 at 0.1 M resulted in a specific capacitance of 583 F/g and an energy density of 80 W h/kg. A specific capacitance of 167.2 F/g was obtained for flower-like CuO-MnO_2 nanosheets prepared by Zhang et al. using the hydrothermal method [20].

Researchers have attempted to enhance the specific capacitance of CuO-doped Mn_2O_3 based electrodes using different morphologies, nanoporous structures, large pore volumes, and high-specific-surface-area materials [21]. The electrochemical performance of manganese oxides can be tuned by the crystal structure and morphology [3]. However, little attention has been paid to the use of the simple SILAR method in developing CuO-doped Mn_2O_3 nanostructures.

In this work, in view of the plausible synergistic effect of CuO and Mn_2O_3, we attempted to demonstrate the fabrication of CuO/Mn_2O_3 nanostructured thin films by the facile and inexpensive SILAR method toward electrochemical energy storage application. The charge storing ability of the material was significantly enhanced owing to the formation of CuO/Mn_2O_3 nanostructures on the stainless steel (SS), which exhibited excellent porosity, high stability, and good electrical conductivity. The incorporation of CuO into Mn_2O_3 was advantageous for electrolyte permeation. This can promote the use of the active material by providing several active sites for reaching the electrolyte ions and ultimately enhancing the electrochemical energy storage performance.

2. Experimental details

2.1. Materials

All the analytical-grade chemical reagents used in this study were procured from Sigma Aldrich and used as received.

2.2. Synthesis of CuO-doped Mn_2O_3 nanostructures

CuO-doped Mn_2O_3 nanostructures were fabricated by the facile SILAR method. SS substrates were used to deposit Mn_2O_3 thin films at room temperature. The SS substrates were ultrasonically cleaned for 5 min in each of the following solvents: distilled water, acetone, and absolute ethanol. These substrates were then dried at room temperature. To deposit CuO-doped Mn_2O_3 thin films, 1 mL of 0.1 M $CuSO_4.6H_2O$, 49 mL of 0.1 M $MnSO_4.H_2O$, and 50 mL of 0.1 M NaOH were used. Initially, the SS substrate was dipped in $MnSO_4.H_2O$ for 20 s to allow the adsorption of Mn^{2+} ions. It was cleaned with distilled water for 5 s to remove any loosely bound Mn^{2+} ions. Following this, the SS substrate was dipped in $CuSO_4.6H_2O$ for 20 s to allow the adsorption of Cu^{2+} ions and then cleaned with distilled water. Finally, it was dipped in the NaOH solution and again cleaned with distilled water. These steps were repeated for 40 SILAR cycles to achieve the desired CuO doped Mn_2O_3 thin films. The thin films with 1, 3, and 5 mol % loading of CuO on Mn_2O_3 were obtained by varying precursor stoichiometry. A similar protocol was used to fabricate pure Mn_2O_3 thin films without the copper precursor solution for comparison. The oxidation of metal hydroxide to metal oxide in alkaline solution is simple [22] and the reaction pathway for the formation of Mn_2O_3 and CuO can be represented as follows.

$$MnSO_4 + 2NaOH \rightarrow Mn(OH)_2 + Na_2SO_4 \quad \text{(i)}$$

$$2Mn(OH)_2 + 2OH \rightarrow Mn_2O_3 + 3H_2O \quad \text{(ii)}$$

$$CuSO_4 + 2NaOH \rightarrow Cu(OH)_2 + Na_2SO_4 \quad \text{(iii)}$$

$$Cu(OH)_2 \rightarrow CuO + H_2O \quad \text{(iv)}$$

2.3. Characterization

Crystallographic information was obtained for the prepared samples by a Rigaku Ultima III diffractometer operated at 40 kV and 40 mA with Cu K< radiation (1.54 A°) as a source. The thin films were starched from the SS to analyze XRD. The morphology and elemental composition of the thin films were acquired using scanning electron microscopy (JEOL JSM-7100) and energy dispersive spectroscopy, respectively. The nanostructures of CuO-Mn_2O_3 visualized using a high-resolution transmission electron microscopy (TEM; JEOL, Model JEM-2100).

2.4. Electrochemical measurements

The electrochemical characteristics were studied using a three-electrode system on a CHI 660 electrochemical workstation. As-prepared samples were used as the working electrodes whereas Pt was used as the counter electrode and Ag/AgCl as the reference electrode. A cyclic potential sweep was applied in the range of 0–0.8 V. Electrochemical impedance measurements were carried out between 1 Hz and 100 kHz with an AC amplitude of 10 mV and a bias potential of 0.4 V.

3. Results and discussion

3.1. Morphological and compositional studies

Fig. 1 (a–h) shows SEM images of the pure Mn_2O_3 and CuO-doped Mn_2O_3 thin films. The pure manganese oxide thin film showed rod-like structures with diameters of 20–25 nm and lengths of 100–120 nm (Fig. 1a-b). The morphology of manganese oxide altered upon doping the matrix with copper. The 1% CuO-doped Mn_2O_3 showed spherical nanoparticles about 10 nm in size that formed aggregates a few hundred nanometers in size covering the nanorod-like nanostructures (Fig. 1c-d). Surprisingly, these nanospheres turned into flakes when the CuO-doping amount reached 3% (Fig. 1e-f) [23–25].

The sizes of the nanoflakes were in the range of about 150–200 nm with a thickness of ˜25 nm. On further increasing the dopant concentration up to 5%, the morphology comprised very compact nanoflakes of manganese oxides (Fig. 1g-h). The SEM results clearly show that the morphology of manganese oxide can be altered with the amount of dopant used in the host matrix. The morphologies noted for the nanostructured Mn_2O_3 with a porous structure are very promising [21]. Fig. 1 (i–l) shows the typical EDS results obtained and the inset shows mapping analysis results for the pure Mn_2O_3 and CuO-doped Mn_2O_3 nanostructures [26,27].

The EDS spectra revealed the presence of only Mn, O, and Cu, which proved the purity of the product. The corresponding elemental mapping revealed the good distribution of Mn, O, and Cu on the substrate. Furthermore, Mn_2O_3 nanostructures were uniformly decorated by CuO nanostructures. Hence, almost all of the nanostructures were available to electrolytes for energy storage owing to the presence of convenient diffusion channels [28]. Fig. 2a shows the possible growth mechanism for the formation of different nanostructure such as nanorods, nanoparticle decorated on nanorods, and hexagonal nanoplates on a (SS) substrate. The deposition mechanism of the hexagonal nanoplate-like 3% CuO-doped Mn_2O_3 thin films involved nucleation, growth, and oriented attachment [24,25,27].

To characterize the surface morphology and nanostructure of the

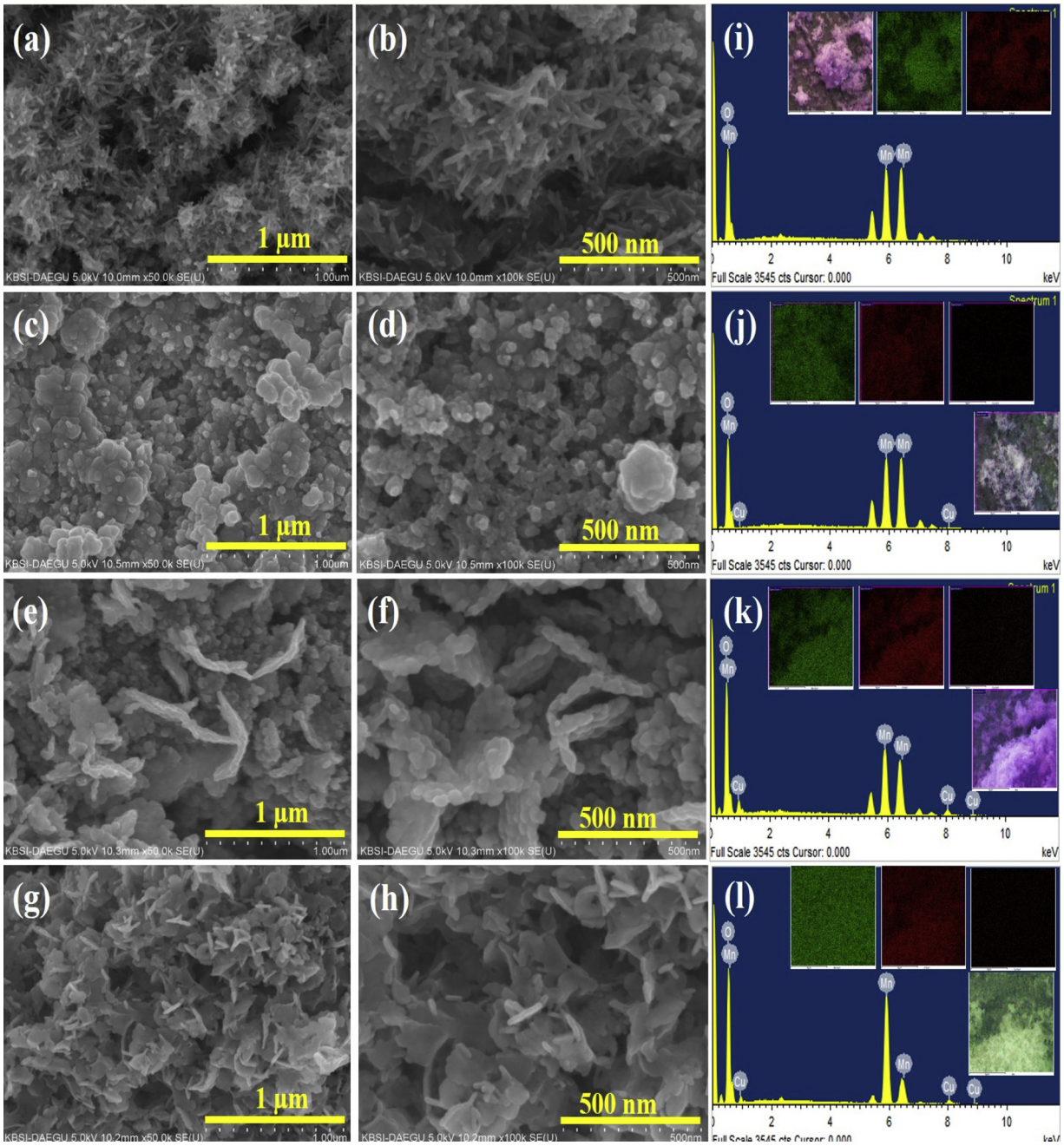

Fig. 1. (a–h) SEM images of Mn_2O_3, 1% CuO-doped Mn_2O_3, 3% CuO-doped Mn_2O_3, and 5% CuO-doped Mn_2O_3 thin films with different magnification, repectively, (i–l) EDS and inset shows the mapping of the Mn_2O_3, 1% CuO-doped Mn_2O_3, 3% CuO-doped Mn_2O_3, and 5% CuO-doped Mn_2O_3 thin films, respectivly.

samples in greater detail, TEM analysis was undertaken at different magnifications. Fig. 2 (b–e) shows the TEM micro images of Mn_2O_3 and CuO-doped Mn_2O_3 thin films: all the samples were fully and uniformly covered with different interconnected 3D nanostructure such as nanorods, nanoparticles, nanoparticles/nanosheets, and hexagonal nanosheets. The high-magnification image of the 3% CuO-doped Mn_2O_3 sample was superior to the other samples in terms of the formation of a porous structure. Such a porous and interconnected nanostructures can allow rapid ion/electron transport, which is very useful for electrochemical applications, especially in a supercapacitor (Fig. 2 (f, g)). The TEM images agreed well with the SEM observations. Fig. 2h reveals the HRTEM results with SEAD patterns and lattice fringes observed for the 3% CuO-doped Mn_2O_3 thin films.

3.2. Structural and electrochemical studies

Fig. 3a depicts the XRD patterns obtained for pure Mn_2O_3 and CuO-doped Mn_2O_3 nanostructures. XRD patterns characteristic of Mn_2O_3 (JCPDS 00-006-0540) were observed for all samples. The diffraction peaks for Mn_2O_3 nanostructures were observed at 28.70°, 32.10°, 35.86°, 50.46°, 58.28°, and 59.83° and they could be assigned to the (202), (221), (203), (115), (510), and (305) planes, respectively. The XRD peaks at 32.10°, 35.86°, and 37.86°, confirmed the presence of copper oxide in the doped manganese oxide samples and matched with the standard XRD peaks of monoclinic CuO (JCPDS 00-048-1548). From these results, we confirmed that the phase formation of CuO/Mn_2O_3 composite after doping of CuO. The absence of other peaks signified high purity of the samples. The remaining diffraction peaks found at 43.23, 50.97, and 74.16 are due to the SS and matched with the 304-

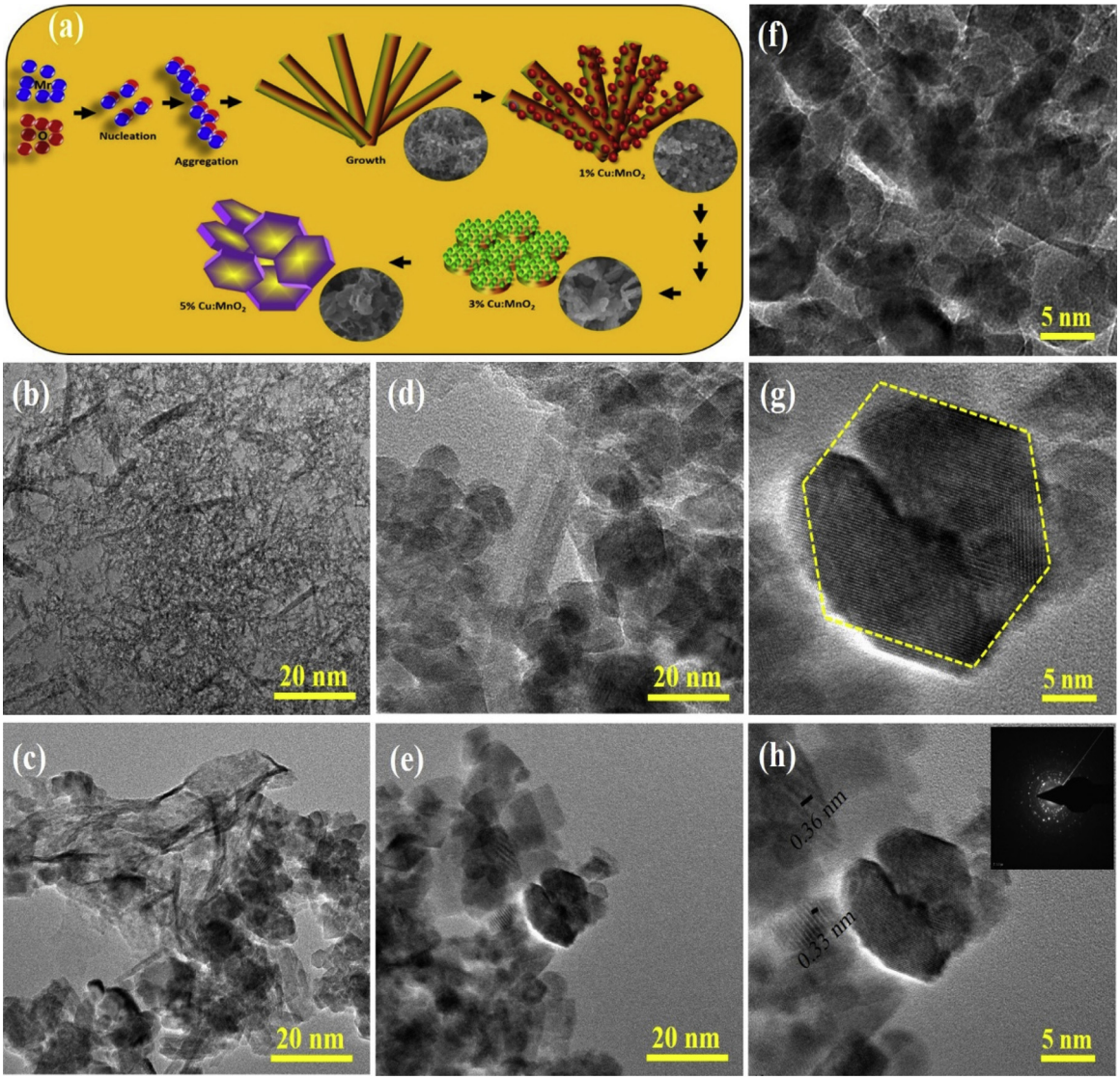

Fig. 2. (a) Schematic of growth formation of CuO-doped Mn_2O_3 thin films using SILAR method, (b–e) TEM images of Mn_2O_3, 1% CuO-doped Mn_2O_3, 3% CuO-doped Mn_2O_3, and 5% CuO-doped Mn_2O_3 thin films, respectivly, (f, g) High magnificed images of 3% CuO-doped Mn_2O_3 thin films, and (h) HRTEM of 3% CuO-doped Mn_2O_3 thin films and inset shows the SEAD patterns of 3% CuO-doped Mn_2O_3 sample, repectively.

stainless steel (JCPDS 00-033-0397) while the peak at 44.20 matches with 434-L stainless steel (JCPDS 00-034-0396) [29,30]. The crystallite size of all samples was estimated using Debye-Scherrer method. The crystallite for undoped Mn_2O_3, 1%, 3% and 5% CuO doped samples are 44.32, 44.31, 27.71, and 36.93 nm, respectively.

The CV profiles of the pure Mn_2O_3 and CuO-doped Mn_2O_3 electrodes (Fig. 3b and S1) show almost symmetrical rectangular shapes in the potential window of 0–0.8 V. The CV profile acquired for the 3% CuO-doped Mn_2O_3 sample was slightly better than that for the 5% CuO-doped Mn_2O_3 one. The current response of 3% CuO-doped Mn_2O_3 increased with an increase in the scan rate, representing good capacitive performance of the electrode (Fig. 3b). In this case, the CV curves maintained the rectangular shape at all scan rates. Fig. 3b shows CV curves obtained for the 3% CuO-doped Mn_2O_3 thin films at different scan rates of 5–100 mV/s in a 3 M KOH electrolyte in the potential window 0.0–0.8 V. The CV curves show an increase in the current density up to 15.33 mA/cm^2 with an increase in the scan rate from 5 to 100 mV/s. Fig. 3b shows that the oxidation and reduction peaks were mirror images of each other for all scan rates, which indicates typical pseudocapacitive behavior. The specific capacitance (C_s) values were estimated according to Eq. (1) [31];

$$C_s = \frac{I}{mv(V_{max} - V_{min})} \int_{V\,min}^{V\,max} I(V)dv \quad (1)$$

where C_s is the specific capacitance, v is the potential scan rate, (V_{max}-V_{min}) is the operating potential window, I is the current density, and m is the deposited mass of active material. The active mass of loading for pure Mn_2O_3, 1% CuO-doped Mn_2O_3, 3% CuO-doped Mn_2O_3, and 5% CuO-doped Mn_2O_3 electrodes were found to be, 0.51, 0.53, 0.47 and 0.45 mg/cm^2, respectively. The value of C_s obtained from the CV curves was calculated to be 500 F/cm^2 at the scan rates of 5–100 mV/s. The enhancement in the capacitive performance of Mn_2O_3 containing 3% CuO could be attributed to the extremely porous nanostructures, which simplified the movement of ions and electrons through the porous structure [20]. The dependence of the specific capacitance on the scan rate (Fig. 3c) resulted in the sample retaining 60% of its initial specific capacitance (from 500 to 300 F/cm^2) as the scan rate increased from 5 to 100 mV/s. This superior rate capability can be related to various factors such as the porous nature of material, an appropriate amount of a suitable dopant, compact diffusion path of ions, easy contact between electrolyte ions, and high electrical conductivity of the nanostructures [32,33].

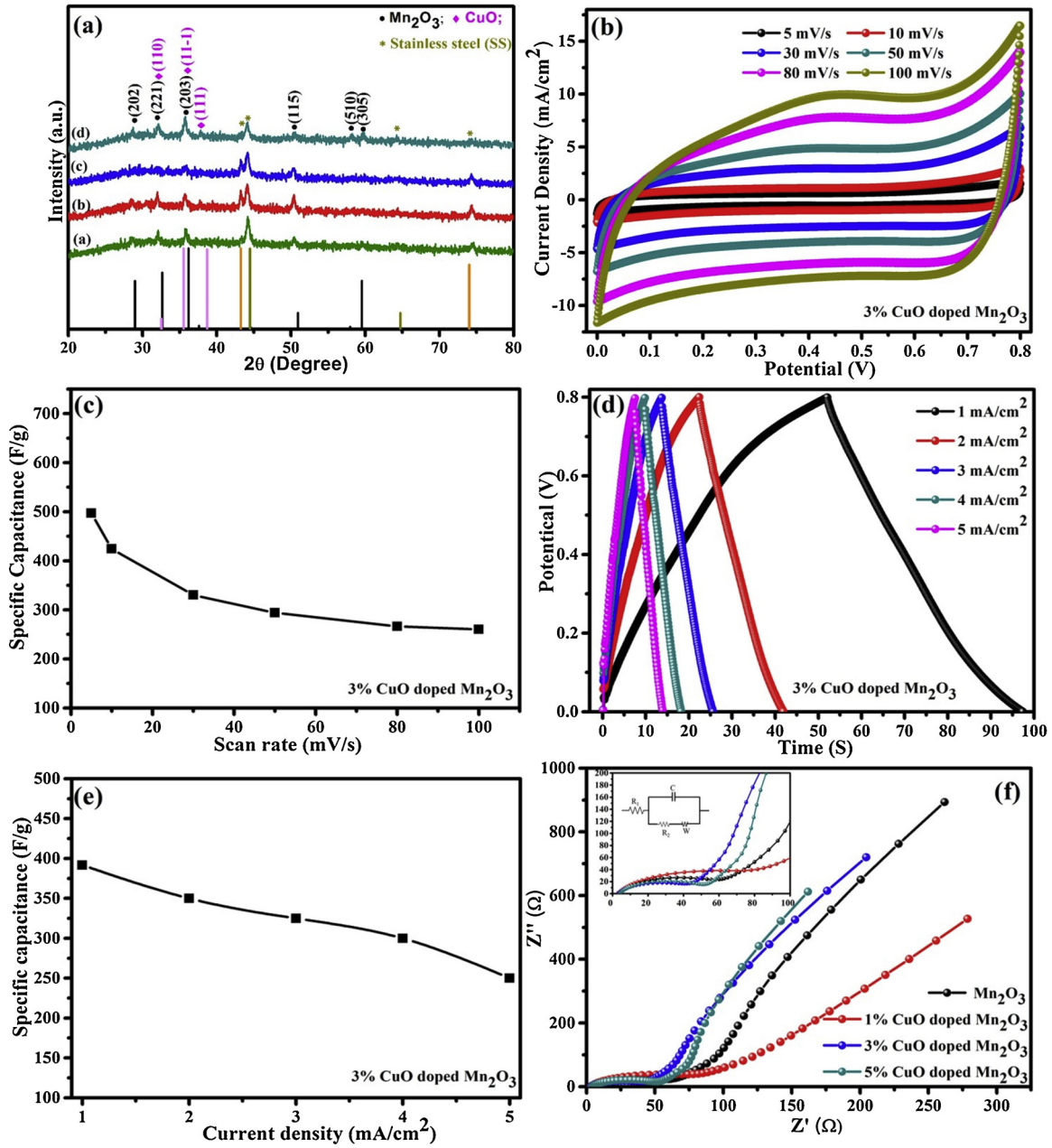

Fig. 3. (a) XRD patterns of Mn_2O_3, 1% CuO-doped Mn_2O_3, 3% CuO-doped Mn_2O_3, and 5% CuO-doped Mn_2O_3 thin films prepered using SILAR method, repectively, (b) CV of the 3% CuO-doped Mn_2O_3 thin films at different scan rate from 5 to 100 mV/s, (c) Specific capactance of the 3% CuO-doped Mn_2O_3 thin films with respect to the scan rate, (d) Galvanostatic charge-discharge of the 3% CuO-doped Mn_2O_3 thin films at different current density from 1 to 5 mA/cm^2, (e) Specific capactance of the 3% CuO-doped Mn_2O_3 thin films with respect to the different current density, respectivly, (f) Nyquist plots of the Mn_2O_3, 1% CuO-doped Mn_2O_3, 3% CuO-doped Mn_2O_3, and 5% CuO-doped Mn_2O_3 thin films, and inset shows the equivalent circuit.

The galvanostatic charge–discharge behavior illustrates that the capacitance performance of Mn_2O_3 improved with increase in the amount of CuO dopant in the host matrix. However, the 3% CuO-doped Mn_2O_3 showed a slightly higher capacitance value than that of the 5% CuO-doped Mn_2O_3, as shown in Fig. 3d and S2. This can be attributed to the spongy and porous morphology of 3% CuO-doped Mn_2O_3 and the compact morphology of the 5% CuO-doped manganese. The galvanostatic charge–discharge measurements were carried out to evaluate the electrochemical performance of the 3% CuO-doped Mn_2O_3 electrode at 0–0.8 V and different current densities (1, 2, 3, 4, and 5 mA/cm^2, Fig. 3d). The charge curve of 3% CuO-doped Mn_2O_3 was identical to its corresponding discharge curve with a minor bend, directing the high reversibility of the hybrid materials [20,34,35]

The *Cs* values were estimated from the GCD curves according to Eq. (2)

$$C_s = \frac{I \times \Delta t}{m \times \Delta V} \quad (2)$$

where *I*, Δt, *m* and ΔV are discharge current (A), discharge time (s), mass of the electrode (cm^2), and discharge potential range (V), respectively. The specific capacitance obtained from the discharging curves was calculated to be 391 F/cm^2 at the current density of 1 mA/cm^2 (Fig. 3e). The highly porous nature of the nanostructures was responsible for the enhanced capacitive performance of the 3% CuO-doped Mn_2O_3 sample. The porous nanostructures helped the migration of ions and electrons[20]. The values obtained in this work are superior to those previously reported (Table 1) [36].

Electrochemical impedance spectroscopy (EIS) spectra of the pure

Table 1
Comparative study of supercapacitor with various methods and nanostructure.

Compounds	Method	Nanostructures	Electrolyte	Specific capacitance	Reference
Cu doped MnO_2	Hydrothermal	Nanosheets	1 M Na_2SO_4	296 F/g at 1 A/g	[2]
Ni doped MnO_2	Simple reaction	Nanosheets	1 M Na_2SO_4	445 F/g at 1 A/g	[8]
Cu doped MnO_2	Chemical precipitation	Nanorods	0.5 M KCl	583 F/g at 10 A/g	[11]
CuO/MnO_2	Hydrothermal	Dandelions	1 M Na_2SO_4	228 F/g	[18]
MnO_2/CuO	Hydrothermal	Nanosheets/flower	1 M Na_2SO_4	167.2 F/g at 0.3 A/g	[20]
CuO/MnO_2	hydrothermal	Diatom	1 M Na_2SO_4	240 F/g at 0.5 A/g	[39]
CuO doped Mn_2O_3	SILAR	Hexagonal nanosheets	3 M KOH	500 F/g	Present study

manganese oxide and CuO-doped Mn_2O_3 were recorded in the range of 1–10^6 Hz. Fig. 3f shows the Nyquist plots of all the samples: it shows a semicircle at high frequencies and a straight line at low frequencies (inset, Fig. 3f). An almost vertical line represents quick ion diffusion in the electrolyte and represents model capacitive performance in the charge–discharge process. The 3% CuO-doped Mn_2O_3 electrode showed good kinetics for the ion diffusion owing to lower mass loading of CuO in the host matrix [37]. The values of solution resistance for the pure Mn_2O_3 and 1%, 3%, 5% CuO-doped Mn_2O_3 were 3.6, 3.1, 2.6, and 3.5 Ω, respectively. The charge transfer resistance of pure Mn_2O_3 and CuO–doped Mn_2O_3 were 59.66, 73.84, 42.27, and 50.91 Ω, respectively. The 3% CuO-doped Mn_2O_3 electrode showed the lowest solution resistance. Meanwhile, its charge transfer resistance also had a lower value than that of other samples, suggesting the electrode was more conductive than the other ones. The higher electric conductivity would lead to faster ion and electron transport in electrochemical reactions [38]. Also, the structural and morphological properties of 3% doped samples are better than that of other samples. The crystallite size of 3% doped sample was lower than other samples which ultimately provide large surface area for electrochemical reactions. Thus, the optimum 3% doped sample shows better electrochemical performance than other samples. Thus, the 3% CuO-doped Mn_2O_3 electrode was chosen for a detailed electrochemical investigation in future.

4. Conclusions

In conclusion, we successfully synthesized CuO-doped Mn_2O_3 nanostructures with different morphologies by the facile and effective SILAR method. The effect of the amount of CuO doped in the Mn_2O_3 on the morphological and electrochemical properties was significant. In particular, 3% CuO-doped Mn_2O_3 showed a high specific capacitance of 500 F/cm^2 at 5 mV/s, demonstrating phase purity, a porous morphology, and good ion diffusion for the electrolyte. An appropriate amount of CuO doped in Mn_2O_3 nanostructures can thus offer promising supercapacitor electrode applications.

Acknowledgment

This study was supported by the Dongguk University Research Fund in the period 2018–2020.

Appendix A. Supplementary data

Supplementary material related to this article can be found, in the online version, at doi:https://doi.org/10.1016/j.colsurfb.2019.110500.

References

[1] P. Simon, Y. Gogotsi, Materials for electrochemical capacitors, Nat. Mater. 7 (2008) 845–854.
[2] X. Su, L. Yu, G. Cheng, H. Zhang, M. Sun, L. Zhang, J. Zhang, Controllable hydrothermal synthesis of Cu-doped δ-MnO_2 films with different morphologies for energy storage and conversion using supercapacitors, Appl. Energy 134 (2014) 439–445.
[3] M. Xu, L. Kong, W. Zhou, H. Li, Hydrothermal Synthesis and Pseudocapacitance Properties of α-MnO_2 Hollow Spheres and Hollow Urchins, Phys. Chem. C 111 (2007) 19141–19147.
[4] M. Aghazadeh, M.R. Ganjali, Evaluation of supercapacitive and magnetic properties of Fe_3O_4 nano-particles electrochemically doped with dysprosium cations: Development of a novel iron-based electrode, Ceram. Int. 44 (2018) 520–529.
[5] M. Aghazadeh, M.G. Maragheh, M.R. Ganjali, P. Norouzi, F. Faridbod, Electrochemical preparation of MnO_2 nanobelts through pulse base-electrogeneration and evaluation of their electrochemical performance, Appl. Surf. Sci. 364 (2016) 141–147.
[6] M. Aghazadeh, M. Hosseinifard, B. Sabour, S. Dalvand, Pulse electrochemical synthesis of capsule-like nanostructures of Co_3O_4 and investigation of their capacitive performance, Appl. Surf. Sci. 287 (2013) 187–194.
[7] M. Aghazadeh, Synthesis, characterization, and study of the supercapacitive performance of NiO nanoplates prepared by the cathodic electrochemical deposition-heat treatment (CED-HT) method, J. Mater. Sci. Mater. Electron. 28 (2017) 3108–3117.
[8] J. Li, Y. Ren, S. Wang, Z. Ren, J. Yu, Transition metal doped MnO_2 nanosheets grown on internal surface of macroporous carbon for supercapacitors and oxygen reduction reaction electrocatalysts, Appl. Mater. Today. 3 (2016) 63–72.
[9] D.J. Davis, T.N. Lambert, J.A. Vigil, M.A. Rodriguez, M.T. Brumbach, E.N. Coker, S.J. Limmer, Role of Cu-ion doping in Cu-α-MnO_2 nanowire electrocatalysts for the oxygen reduction reaction, J. Phys. Chem. C 118 (2014) 17342–17350.
[10] M. Huang, Y. Zhang, F. Li, Z. Wang Alamusi, N. Hu, Z. Wen, Q. Liu, Merging of kirkendall growth and ostwald ripening: CuO@MnO_2 core-shell architectures for asymmetric supercapacitors, Sci. Rep. 4 (2015) 4518, https://doi.org/10.1038/srep04518.
[11] R. Poonguzhali, R. Gobi, N. Shanmugam, A. Senthil Kumar, G. Viruthagiri, N. Kannadasan, Enhancement in electrochemical behavior of copper doped MnO_2 electrode, Mater. Lett. 157 (2015) 116–122.
[12] H. Yu, X. Rui, H. Tan, J. Chen, X. Huang, C. Xu, W. Liu, D.Y.W. Yu, H.H. Hng, H.E. Hoster, Q. Yan, Cu doped V_2O_5 flowers as cathode material for high-performance lithium ion batteries, Nanoscale 5 (2013) 4937.
[13] K. Qian, Z. Qian, Q. Hua, Z. Jiang, W. Huang, Structure–activity relationship of CuO/MnO_2 catalysts in CO oxidation, Appl. Surf. Sci. 273 (2013) 357–363.
[14] V. Di Castro, C. Furlani, M. Gargano, M. Rossi, XPS characterization of the CuO/MnO_2 catalyst, Appl. Surf. Sci. 28 (1987) 270–278.
[15] A. Martin, U. Armbruster, M. Schneider, J. Radnik, M.-M. Pohl, Structural transformation of an alumina-supported MnO_2–CuO oxidation catalyst by hydrothermal impact of sub- and supercritical water, J. Mater. Chem. 12 (2002) 639–645.
[16] X. Tong, L. Yu, H. Chen, X. Zhuang, S. Liao, H. Cui, Highly efficient and selective oxidation of 5-hydroxymethylfurfural by molecular oxygen in the presence of Cu-MnO_2 catalyst, Catal. Commun. 90 (2017) 91–94.
[17] S.K. Shinde, D.P. Dubal, G.S. Ghodake, V.J. Fulari, Electronic impurities (Fe, Mn) doping in CdSe nanostructures for improvements in photoelectrochemical applications, RSC Adv. 4 (2014) 33184.
[18] Z. Zhang, C. Ma, M. Huang, F. Li, S. Zhu, C. Hua, L. Yu, H. Zheng, X. Hu, Y. Zhang, Birnessite MnO_2-decorated hollow dandelion-like CuO architectures for supercapacitor electrodes, J. Mater. Sci. Mater. Electron. 26 (2015) 4212–4220.
[19] H. Chen, M. Zhou, T. Wang, F. Li, Y.X. Zhang, Construction of unique cupric oxide–manganese dioxide core–shell arrays on a copper grid for high-performance supercapacitors, J. Mater. Chem. A 4 (2016) 10786–10793.
[20] Y. Xin Zhang, F. Li, M. Huang, One-step hydrothermal synthesis of hierarchical MnO_2-coated CuO flower-like nanostructures with enhanced electrochemical properties for supercapacitor, Mater. Lett. 112 (2013) 203–206.
[21] G. Yu, L. Hu, N. Liu, H. Wang, M. Vosgueritchian, Y. Yang, Y. Cui, Z. Bao, Enhancing the supercapacitor performance of Graphene/MnO_2 nanostructured electrodes by conductive wrapping, Nano Lett. 11 (2011) 4438–4442.
[22] J. Fu, Z. He, H. Wang, W. Liang, C. Guo, Preparation of chemical manganese dioxide from manganese sulfate, Min. Sci. Technol. 20 (2010) 877–881.
[23] S. Shinde, H. Dhaygude, D.-Y. Kim, G. Ghodake, P. Bhagwat, P. Dandge, V. Fulari, Improved synthesis of copper oxide nanosheets and its application in development of supercapacitor and antimicrobial agents, J. Ind. Eng. Chem. 36 (2016) 116–120.
[24] S.K. Shinde, D.P. Dubal, G.S. Ghodake, D.Y. Kim, V.J. Fulari, Nanoflower-like CuO/$Cu(OH)_2$ hybrid thin films: Synthesis and electrochemical supercapacitive properties, J. Electroanal. Chem. 732 (2014) 80–85.
[25] S.K. Shinde, D.P. Dubal, G.S. Ghodake, V.J. Fulari, Hierarchical 3D-flower-like CuO nanostructure on copper foil for supercapacitors, RSC Adv. 5 (2015) 4443–4447.
[26] S.K. Shinde, V.J. Fulari, D.-Y. Kim, N.C. Maile, R.R. Koli, H.D. Dhaygude, G.S. Ghodake, Chemical synthesis of flower-like hybrid $Cu(OH)_2$/CuO electrode: Application of polyvinyl alcohol and triton X-100 to enhance supercapacitor performance, Colloids Surf. B Biointerfaces 156 (2017) 165–174.
[27] S.K. Shinde, D.P. Dubal, G.S. Ghodake, V.J. Fulari, Morphological modulation of Mn:CdSe thin film and its enhanced electrochemical properties, J. Electroanal.

Chem. 727 (2014) 179–183.
[28] Q. Chen, B. Heng, H. Wang, D. Sun, B. Wang, M. Sun, S. Guan, R. Fu, Y. Tang, Controlled facile synthesis of hierarchical CuO@MnO_2 core–shell nanosheet arrays for high-performance lithium-ion battery, J. Alloys Compd. 641 (2015) 80–86.
[29] M. Dadfar, M.H. Fathi, F. Karimzadeh, M.R. Dadfar, A. Saatchi, Effect of TIG welding on corrosion behavior of 316L stainless steel, Mater. Lett. 61 (2007) 2343–2346.
[30] S. Lee, E.-W. Huang, W. Woo, C. Yoon, H. Chae, S.-G. Yoon, Dynamic strain evolution around a crack tip under steady- and overloaded-fatigue conditions, Metals (Basel) 5 (2015) 2109–2118.
[31] S.K. Shinde, G.S. Ghodake, V.J. Fulari, D.-Y. Kim, High electrochemical performance of nanoflakes like CuO electrode by successive ionic layer adsorption and reaction (SILAR) method, J. Ind. Eng. Chem. 52 (2017) 12–17.
[32] S.K. Shinde, M.B. Jalak, G.S. Ghodake, N.C. Maile, H.M. Yadav, A.D. Jagadale, A. Shahzad, D.S. Lee, A.A. Kadam, V.J. Fulari, D.-Y. Kim, Flower-like $NiCo_2O_4$/$NiCo_2S_4$ electrodes on Ni mesh for higher supercapacitor applications, Ceram. Int. (2019).
[33] S.K. Shinde, H.M. Yadav, G.S. Ghodake, A.A. Kadam, V.S. Kumbhar, J. Yang, K. Hwang, A.D. Jagadale, S. Kumar, D.Y. Kim, Using chemical bath deposition to create nanosheet-like CuO electrodes for supercapacitor applications, Colloids Surf. B Biointerfaces 181 (2019) 1004–1011.
[34] S.K. Shinde, M.B. Jalak, G.S. Ghodake, N.C. Maile, V.S. Kumbhar, D.S. Lee, V.J. Fulari, D.-Y. Kim, Chemically synthesized nanoflakes-like $NiCo_2S_4$ electrodes for high-performance supercapacitor application, Appl. Surf. Sci. 466 (2019) 822–829.
[35] S. Ramesh, H.S. Kim, Y. Haldorai, Y.-K. Han, J.-H. Kim, Fabrication of nanostructured MnO_2/carbon nanotube composite from 3D precursor complex for high-performance supercapacitor, Mater. Lett. 196 (2017) 132–136.
[36] A. Kathalingam, S. Ramesh, A. Sivasamy, H.-S. Kim, H.-S. Kim, Supercapacitor performance of MnO_2/$NiCo_2O_4$@N-MWCNT hybrid nanocomposite electrodes, J. Sol-Gel Sci. Technol. 91 (2019) 154–164.
[37] W. Xu, S. Dai, G. Liu, Y. Xi, C. Hu, X. Wang, CuO nanoflowers growing on carbon fiber fabric for flexible high-performance supercapacitors, Electrochim. Acta 203 (2016) 1–8.
[38] S.K. Shinde, G.S. Ghodake, D.P. Dubal, H.D. Dhaygude, D.-Y. Kim, V.J. Fulari, Enhanced photoelectrochemical properties of nanoflower-like hexagonal $CdSe_{0.6}Te_{0.4}$: Effect of electron beam irradiation, J. Ind. Eng. Chem. 45 (2017) 92–98.
[39] Y. Zhang, W.W. Guo, T.X. Zheng, Y.X. Zhang, X. Fan, Engineering hierarchical Diatom@CuO@MnO_2 hybrid for high performance supercapacitor, Appl. Surf. Sci. 427 (2018) 1158–1165.